OPEN ACCESS

Effect of Fe–N–Cs as Catalytic Active Support for Platinum towards ORR in Acidic Environment

To cite this article: Dana Schonvogel *et al* 2023 *J. Electrochem. Soc.* **170** 114518

Journal of The Electrochemical Society, 2023 **170** 114518

Effect of Fe–N–Cs as Catalytic Active Support for Platinum towards ORR in Acidic Environment

Dana Schonvogel,[z] Nambi Krishnan Nagappan, Julia Müller-Hülstede, Nina Bengen, and Peter Wagner

German Aerospace Center (DLR), Institute of Engineering Thermodynamics, 26129 Oldenburg, Germany

Metal-nitrogen-carbon (M–N–C) compounds such as Fe–N–Cs are currently the most promising platinum group metal free catalysts for oxygen reduction in acidic environment. Regarding the overriding goal of reducing PEMFC production costs by reducing the platinum content, the use of Fe–N–Cs as catalytic active support for low Pt amounts is investigated in this study. Activity and stability of Pt in different contents on a commercial Fe–N–C is compared to Pt on a typical carbon black. Pt nanoparticles are well-distributed on both support substrate classes. Although the electrochemical surface and mass activity of Pt is lower on Fe–N–C compared to carbon black, the Fe–N–C has a contribution to total ORR activity depending on the Pt/Fe–N–C ratio, which is quantified. In the low Pt content case of 1 wt%, the ORR activity is increased by factor of two in presence of Fe–N–C. This boosting effect on ORR activity is important for future strategies to lower the Pt content in PEMFCs.
 [DOI: 10.1149/1945-7111/ad09f4]

Manuscript submitted June 26, 2023; revised manuscript received October 18, 2023. Published November 17, 2023.

Supplementary material for this article is available online

Polymer electrolyte membrane fuel cells (PEMFCs) are recognized as one of the renewable energy converters in portable, automobile, and stationary applications. Currently, both low temperature (LT) and high temperature (HT) PEMFCs use platinum group metal (PGM) based catalysts for oxygen reduction reaction (ORR) containing usually Pt nanoparticles on carbon black. To reduce the total cost of a PEMFC stack, worldwide researchers have shown considerable attention to find more inexpensive alternative catalysts and electrodes. Optimized electrode fabrication can lead to enhanced Pt utilization and thus less required Pt amounts in PEMFC. Martinez-Vazquez et al. used electrospray coating and prepared cathode and anode with 0.01 mg_{Pt} cm^{-2}, respectively. They reported a single cell power of 30–35 kW g_{Pt}^{-1}.[1] Pt-alloy catalysts based on PtNi, PtCo or PtFe combinations are known to enhance the ORR activity in acidic environments, which can allow the PGM-content reduction in PEMFCs.[2] Zhao et al. developed a graphene-encaged PtCo catalyst with low cathode loading of 0.06 mg_{Pt} cm^{-2} and 13 kW g_{Pt}^{-1} in LT-PEMFC application.[3] For HT-PEMFC conditions using phosphoric acid at 160 °C, Shroti et al. recently introduced PtCo-alloy particles on multi-walled carbon nanotubes into the cathode and achieved reduced Pt contents by 40% maintaining single cell performance and stability.[4]

Up to now, metal-nitrogen-carbon (M–N–C) compounds such as Fe–N–Cs are the most promising catalysts without using any PGMs for ORR in PEMFC. However, they suffer from insufficient volumetric activity and electrochemical stability in PEMFCs compared to common Pt/C catalysts.[5,6] Fe–N–Cs show degradation during LT-PEMFC operation in terms of iron dissolution and agglomeration, which leads to demetallation of catalytic active Fe-N_x sites and also their loss caused by carbon corrosion.[7–10] Also, reactive oxygen species (ROS) stemming from Fenton reaction of H_2O_2 after two-electron-ORR can attack the carbonic structure and provoke carbon corrosion with active site loss.[10,11] For HT-PEMFCs at constant load operation of 0.1 A cm^{-2}, Müller-Hülstede et al. recently showed Fe-N_x demetallation as main degradation path with negligible carbon corrosion on the one hand and the positive Fe–N–C impact on the phosphoric acid electrolyte distribution in the catalytic layer on the other hand.[12] Liu et al. recently demonstrated Fe–N–C protection from degradation via heat treatment with NH_4Cl and deposition of a thin NC layer on the Fe–N–C catalyst surface. LT-PEMFC testing showed a very low peak power density loss of 4% after 30,000 voltage cycles.[13]

Xiao et al. developed a Pt–Fe–N–C compound consisting of atomically dispersed Pt and Fe and PtFe alloy nanoparticles on a nitrogen-doped graphitic carbon as cathode catalyst. After RDE test with 70,000 potential cycles between 0.6–1.0 V_{RHE}, the ORR half-wave potential was unchanged and proved electrochemical stability of Pt–Fe–N–C. In LT-PEMFC testing at 80 °C using H_2/O_2, this catalyst was compared with Fe-N-C. After 85 h of constant potential of 0.4 V the current loss was 20% compared to 50% after 23 h only for Fe-N-C.[14] Recently, Xiao et al. reported further LT-PEM single cell testing of this Pt-Fe-N-C cathode catalyst at 80 °C using H_2/O_2. A low cathodic Pt loading of 0.015 mg_{Pt} cm^{-2} was chosen. The relative ORR activity was reported to be 97% after 10,000 potential cycles between 0.60–0.95 V_{RHE}.[15] Mechler et al. reported that the addition of 1-2 wt% Pt in hybrid Pt/Fe-N-C catalyst performs well with an increased stability in LT-PEMFCs.[16] It was anticipated that the presence of platinum might chemically reacts with H_2O_2 or ROS, so that less Fe-N-C attacking and loss of active sites takes place. Liao et al. synthesized Pt nanoparticles in presence of self-synthesized resin-based Fe-N-C with a Pt amount of 1.38 wt%. They found a higher mass activity by factor of 1.2 and a higher specific activity by factor of 2.5 compared to a commercial Pt/C.[17] In order to investigate effects of Fe-N-C in Pt-based cathodes for HT-PEMFCs, Müller-Hülstede et al. recently prepared gas diffusion electrodes by physically mixing Fe-N-C and a common PtNi/C cathode catalyst via ultrasonication.[18] Fe-N-C incorporation resulted in phosphoric acid attraction and activity retention, however, due to changed acid distribution effects longer cell activation periods are required.

With the goal of reducing LT- and HT-PEMFC production costs, Pt/Fe-N-C activity and stability with direct precipitation of Pt in systematically reduced contents has not fundamentally been investigated yet. In this study, Pt/Fe-N-C hybrids are synthesized using PMF-011904 from Pajarito Powder (USA) as Pt support and wet-chemically precipitated Pt nanoparticles with targeted Pt-contents of 40, 5 and 1 wt%. This chosen commercial Fe-N-C is the current benchmark and comprehensively characterized in literature.[19,20] To identify the effect of this multiply verified catalytically active Fe-N-C as support,[19,20] Pt/C catalysts are synthesized in the same way using Black Pearls® 2000 (C) from Cabot (United States). Pt contents, electronic structure and morphology as well as particle diameters and distribution on the Fe-N-C and C supports,

[z]E-mail: dana.schonvogel@dlr.de

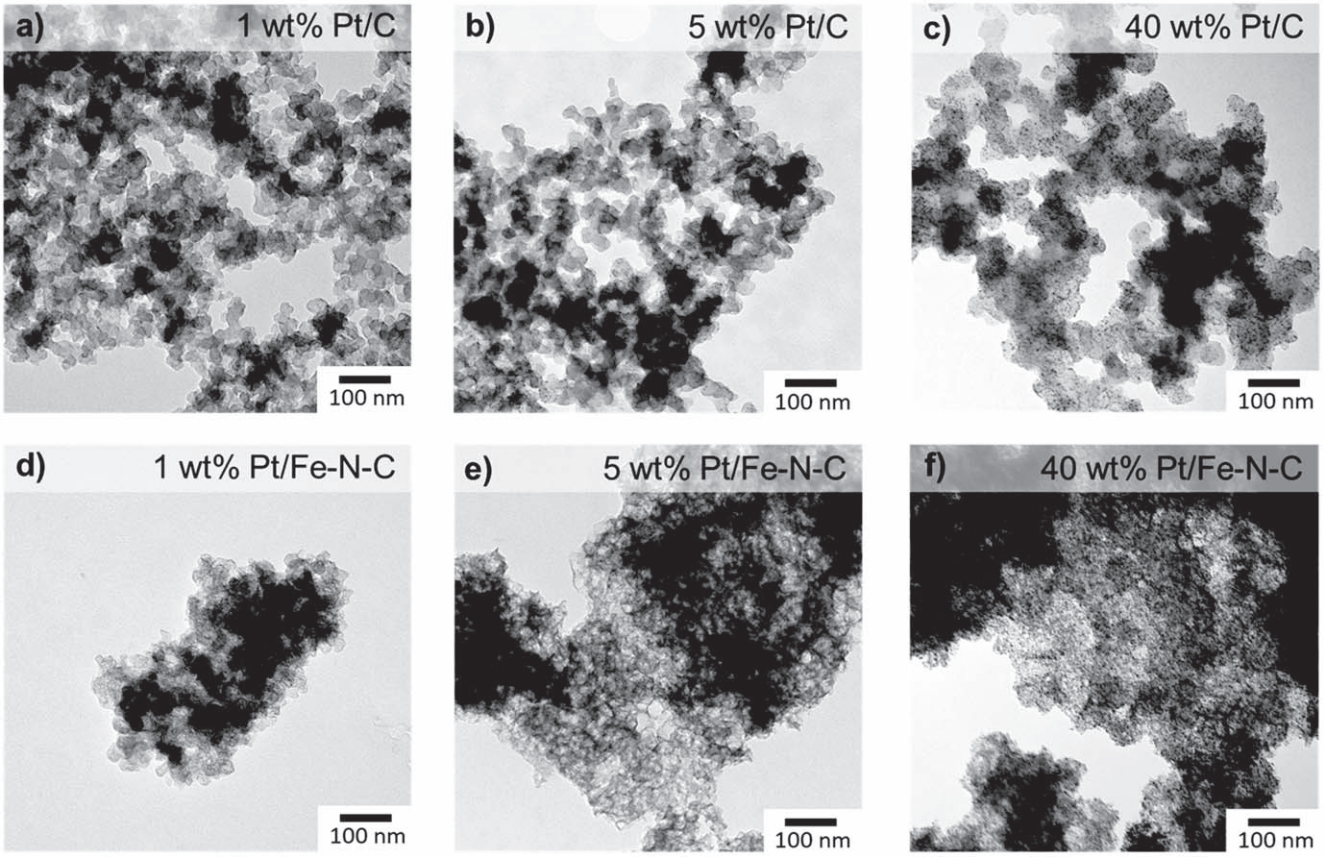

Figure 1. TEM images of catalysts with different Pt contents.

respectively, are investigated by transmission electron microscopy (TEM), scanning TEM with energy dispersive X-ray spectroscopy (EDS), X-ray photoelectron spectroscopy (XPS) and inductively coupled plasma mass spectrometry (ICP-MS) first. Second, mass activity (MA) and specific activity (SA) of ORR are investigated in 0.1 mol l^{-1} $HClO_4$, and the electrochemical surface area (ECSA) of Pt is calculated by hydrogen underpotential deposition and CO stripping voltammetry. Last, accelerated stress testing (AST) is performed with 5,000 triangle potential cycles between 0.6–1.5 V_{RHE} to evaluate the catalyst stability.

Experimental

Catalyst synthesis.—Catalyst supports in this study are Black Pearls® 2000 (C) from Cabot (United States) and PMF-011904 from Pajarito Powder (United States). Both supports were used to deposit Pt nanoparticles in targeted contents of 1 wt%, 5 wt% and 40 wt% each. The synthesis of Pt nanoparticles and their deposition were according to literature.[21–23] 692 mg of $H_2PtCl_6x6H_2O$ from Alfa Aesar (United States) were put in 88 ml of ethylene glycol from Carl Roth (Germany). 12 ml of a NaOH ethylene glycol mixture in a concentration of 2 mol l^{-1} were added to reach an alkaline environment. The mixture was stirred for 4 h at 140 °C to precipitate the nanoparticles. To deposit 40 wt% platinum on the support then, 19.5 ml of nanoparticle suspension were mixed with 40 ml of HCl in a concentration of 1 mol l^{-1} and centrifuged for 10 min at 7000 rpm to separate the nanoparticles. Afterwards, particles were washed three times by using fresh 1 mol l^{-1} HCl solution, and centrifugation was done again. After dispersing the particles in acetone, 60 mg of support was added. To reach the further Pt contents of 1 wt% and 5 wt%, the amount of added support was adapted in an appropriate way. The mixture was then sonicated in a sonification bath until complete acetone evaporation. The final catalyst was dried under vacuum overnight, washed with ultrapure water and dried a second time under vacuum overnight.

Table I. Pt content (measured through ICP-MS) and averaged Pt diameter (measured through TEM).

Catalyst	Pt content/wt%	Pt diameter/nm
1 wt% Pt/C	0.4	—
5 wt% Pt/C	3.8	1.20 ± 0.42
40 wt% Pt/C	38.6	1.22 ± 0.48
1 wt% Pt/Fe-N-C	1.4	—
5 wt% Pt/Fe-N-C	4.0	1.02 ± 0.34
40 wt% Pt/Fe-N-C	38.1	2.02 ± 0.54

Physical characterization.—For TEM the appropriate catalyst powder was dispersed in ethanol, and 5 μl of the dispersion was then dropped onto a copper grid from Plano (Germany) consisting of 200 meshes and being coated with carbon/formvar. Microscopy was then performed using the EM 902 A device from Carl Zeiss (Germany) with a tungsten cathode and a CCD camera and an acceleration voltage of 80 kV. The Pt nanoparticle diameter was measured using the ImageJ software and averaged using at least 300 particles.

For scanning TEM (STEM) with EDS samples from TEM analysis were used. STEM/EDS were recorded with a JEM-2100F from Jeol (Germany) with 80–200 kV accelerating voltage and 250 X-Max80 SDD detector and INCA software from Oxford instruments (United Kingdom).

XPS was recorded at the FEI ESCALAB Xi+ from Thermo Scientific (Germany) equipped with an Al Kα radiation. Samples were deposited on a gold substrate. For survey spectra, 3 scans with

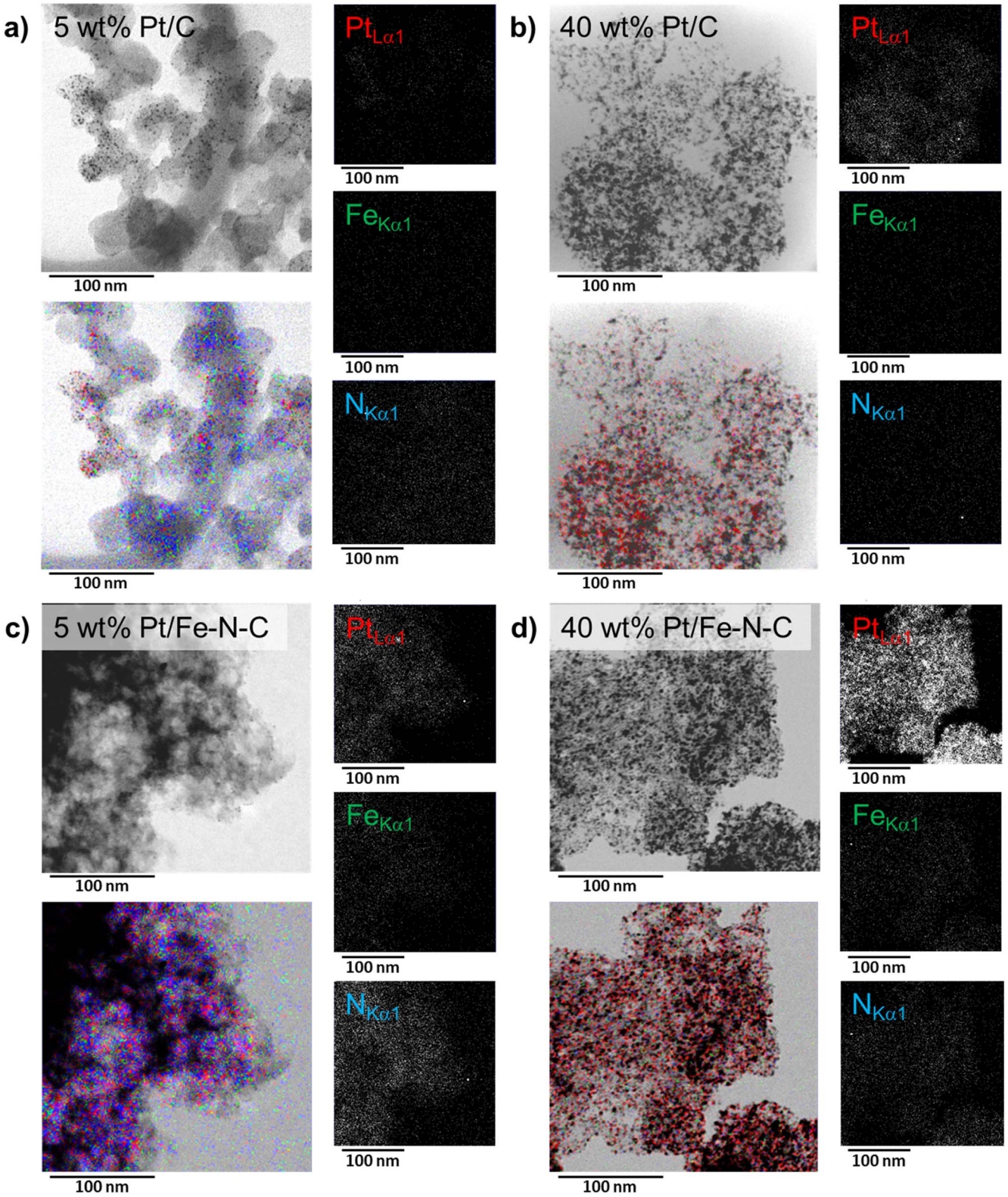

Figure 2. STEM images with EDS mapping of (a) 5 wt% Pt/C, (b) 40 wt% Pt/C, (c) 5 wt% Pt/Fe-N-C and (d) 40 wt% Pt/Fe-N-C.

a pass energy of 100 eV, dwell time of 10 ms, and step size 0.5 eV were averaged. For high resolution spectra, the following parameter (scans; pass energy; dwell time; step size) were used: Fe2p (30; 50 eV; 100 s; 0.1 eV), O1s (10; 20 eV; 100 s; 0.1 eV), N1s and C1s (20; 20 eV; 100 s; 0.05 eV) and Pt4f (50; 20 eV; 100 s; 0.05 eV). For each material with exception of 1 wt% Pt/Fe-N-C two positions were measured and evaluated. Spectra were fitted using the Avantage software from Thermo Scientific (Germany) and smart background and Gauss-Lorentz line shape.

For ICP-MS, 2 mg of catalyst powder was stored overnight in 1.6 ml concentrated HCl from Carl Roth (Germany) and 1.3 ml concentrated HNO_3 from Carl Roth (Germany) to dissolve platinum.

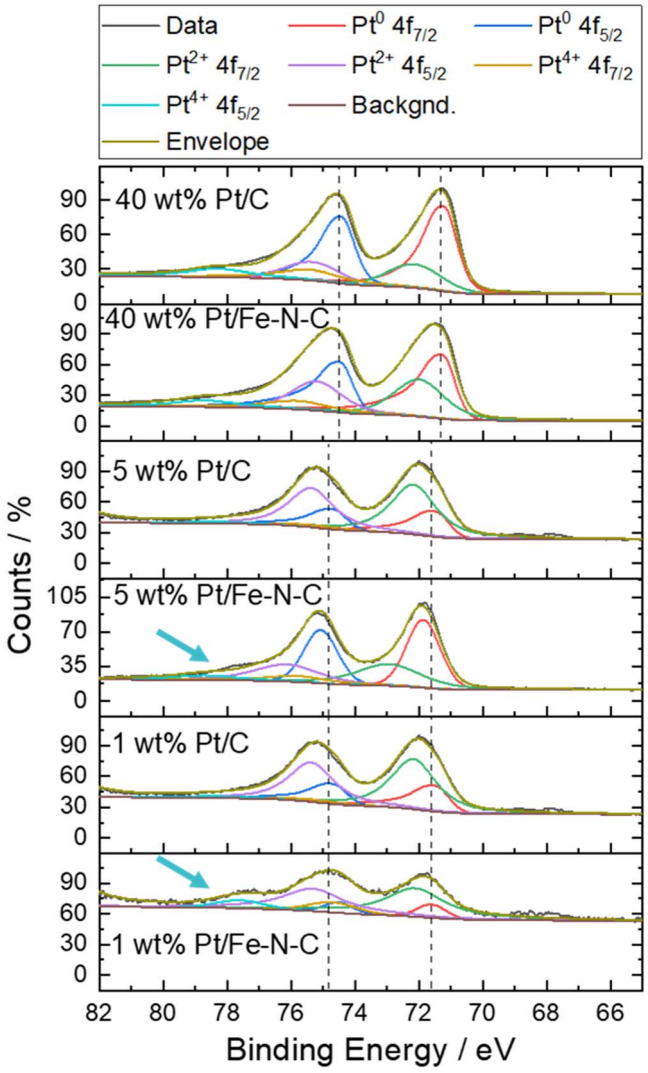

Figure 3. High resolution XPS of Pt4f.

Then, the mixture was filtered and diluted using 2 wt% HNO_3 to reach a final volume of 250 ml and the final acidification with nitric acid. Lu ICP standard from Carl Roth (Germany) was added to a final internal standard concentration of 1 mg l^{-1}. Pt calibration solutions containing 100, 200, 300, 400, 600 and 800 μg l^{-1} were prepared using a Pt ICP standard from Carl Roth (Germany). The measurement was performed using the XSeries2 device from Thermo Fisher Scientific (Germany). During calibration a correlation factor of at least 0.999 was ensured, and signal intensities of the ^{194}Pt, ^{195}Pt and ^{196}Pt isotopes were used to calculate the Pt concentrations.

Electrochemical characterization.—To electrochemically characterize and compare the catalysts of this study, rotating disc electrodes (RDEs) with a glassy carbon disc consisting of an area of 0.2475 cm^2 from Pine were used in a three-electrode setup. While the reference electrode was the reversible hydrogen electrode (RHE) of the type HydroFlex from Gaskatel (Germany), a platinum wire was used as counter electrode. This three-electrode setup was connected to the Autolab PGSTAT128N potentiostat from Metrohm (Germany) equipped with the Nova 2.1 software to perform electrochemical measurements of three identically prepared RDEs for each catalyst.

Therefore, these electrodes were polished by aluminum oxide particle suspensions of the type MicroPolish 40–10081 from Bühler (Switzerland) with particle diameters of 1.00 μm first and 0.05 μm second and then coated with appropriate catalyst suspensions. These suspensions consist of 6 mg of catalyst powder, 1.99 ml H_2O, 0.5 ml 2-propanol and 20 μl of 5 wt% Nafion® in aliphatic alcohol and water dispersion from Sigma Aldrich (Germany). To achieve a homogenous suspension sonication was used for 15 min in a sonication bath and by horn-sonication for 4 min (intervals of 30 s switched on and 30 s switched off). A volume of 10.3 μl of suspension was dropped on the RDE which was then rotated using 700 rpm for drying and final coating with 100 μg cm^{-2} of total catalyst amount to keep the coating amount constant independent of the Pt content in the different catalysts. Perchloric acid from Sigma Aldrich (Germany) in a concentration of 0.1 mol l^{-1} presented the electrolyte during these measurements. Measurements were then carried out using the following procedure.

First, the electrolyte was rinsed with N_2 for 15 min for saturation. Second, cyclic voltammetry (CV) at 0.05–1.20 V_{RHE} with a scan rate of 0.5 V s^{-1} was performed until a steady-state was achieved. Third, the initial characterization was done. This included three CV curves at 0.05–1.05 V_{RHE} with a scan rate of 0.05 V s^{-1} to determine the ECSA later and further three CV curves at 0.05–1.15 V_{RHE} with a scan rate of 0.005 V s^{-1} to carry out capacitive background corrections later. After CV, CO stripping voltammetry was carried out. Therefore, the electrolyte was purged with CO for 1 min and with N_2 for 20 min during applying a constant potential of 0.15 V_{RHE} to record afterwards a CV curve at 0.05-0.3 V_{RHE} with a scan rate of 0.05 V s^{-1}. This verified complete Pt surface poisoning. Then, the actual CO stripping took place by CV at 0.15–1.05 V_{RHE} with a scan rate of 0.05 V s^{-1}. After CO stripping, electrochemical impedance spectroscopy recorded at 0.5 V_{RHE} in range of 100 kHz–0.1 Hz was applied to measure the electrolyte resistance for ORR curve correction. For following ORR, the electrolyte was rinsed with O_2 for 20 min followed by recording three CV curves during rotation using 1600 rpm. CV was performed at 0.05–1.15 V_{RHE} with a scan rate of 0.005 V s^{-1}.

After this initial characterization, the electrolyte was rinsed again using N_2 for 20 min to apply an accelerated stress test (AST). This included 5000 cycles between 0.6–1.5 V_{RHE} with a scan rate of 0.5 V s^{-1}. Last, the characterization above was repeated at the end of the procedure to assess catalyst degradation or stability. ECSAs and mass activities were calculated by considering the three identically measured electrodes in each case according to our previous studies.[24,25]

Results and Discussion

Morphology and elemental composition.—Figure 1 depicts TEM images of the six catalysts with different Pt contents and supports in comparison. Due to low Pt contents the 1 wt% and 5 wt% Pt catalysts mainly show the support morphologies under the microscope, whereas the 40 wt% Pt catalysts show well-distributed Pt nanoparticles on the supports. This verifies sufficient interaction of the Pt nanoparticles with the support in both cases. Next to distributed Pt nanoparticles differences in support morphologies become visible. While Black Pearls (C) consist of the typical carbon particles with diameters of 10–40 nm resulting in larger aggregates, PMF (Fe-N-C) has a more visible inner-porous structure.

Table I shows the Pt content of all catalysts analyzed by ICP-MS and the averaged diameters of Pt nanoparticles analyzed by TEM. ICP-MS reveals values slightly lower than the targeted content in most cases and a larger value than the targeted content in case of 1 wt% Pt/Fe-N-C. The trend of increasing Pt contents from 1 wt% to 5 wt% and 40 wt% is clearly visible for both supports C and Fe-N-C, so that the impact of support and of increasing Pt contents on the ECSA and the ORR can be investigated via electrochemical characterization below. There, the real Pt amounts from this Table I are considered during determination of ECSAs and mass activities for ORR below and ensure high comparability of these electrochemical results. Averaged diameters of Pt nanoparticles are analyzed by TEM for 5 wt% and 40 wt% catalysts and are compared

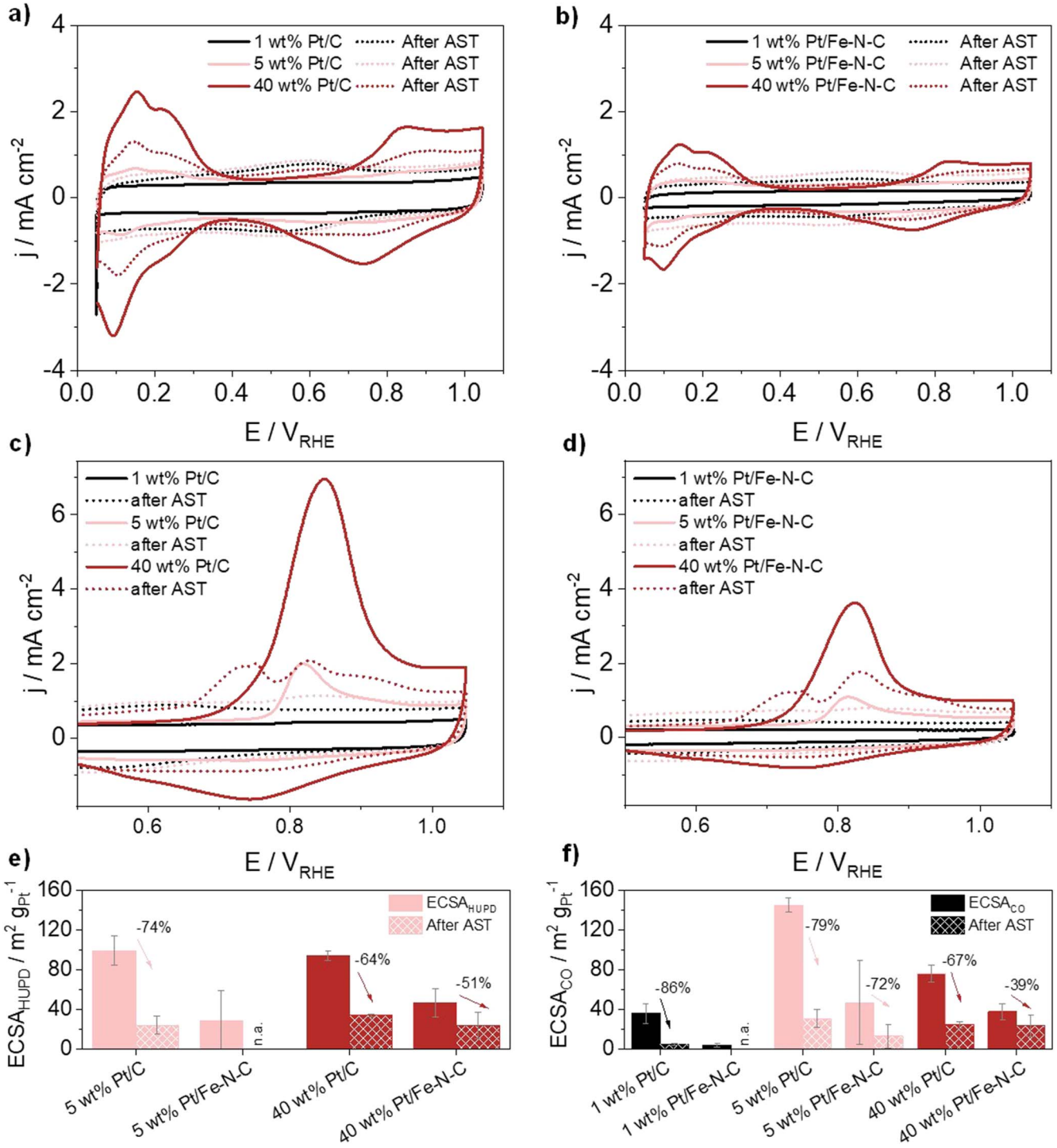

Figure 4. (a), (b) CVs for determination of $ECSA_{HUPD}$ with (e) corresponding ECSA values, and c,d) CO stripping voltammetry for determination of $ECSA_{CO}$ with (f) corresponding ECSA values before and after AST (5,000 cycles, 0.6–1.5 V_{RHE} with 0.5 V s^{-1}, N_2-saturated $HClO_4$).

in Table I. The 1 wt% catalysts contain very little platinum verified by ICP-MS. The very few Pt nanoparticles being visible under microscope make the determination of nanoparticle diameters not feasible. The 5 wt% Pt catalysts show diameters of about 1.20 nm and 1.02 nm, and the 40 wt% Pt catalysts show diameters of about 1.22 nm and 2.02 nm which is the typical range expected from the polyol synthesis in previous studies.[24,26]

In addition, STEM measurements with EDS are shown in Fig. 2 for 5 wt% and 40 wt% pt catalysts, since Pt nanoparticles are clearly visible for these catalysts. The elemental distribution of Pt, Fe and N in comparison shows the following trends. Figures 2c and 2d of 5 wt% and 40 wt% Pt/Fe-N-C show a larger detection of Fe and N than each related Pt/C catalyst. This indicates the expected higher Fe-/N-contents within the carbon network of commercial PMF compared to carbon black. Furthermore, Fe- or N-containing particles are not visible, so that Fe and N are expected to be atomically incorporated into the graphitic carbon. This is known for the commercial PMF catalyst.[19,20] Here, it is proven that no morphological change and particle formation took place within PMF through Pt precipitation. Regarding Pt, Figs. 2b and 2d with 40 wt% Pt catalysts show the expected detection of more Pt nanoparticles compared to the 5 wt% cases.

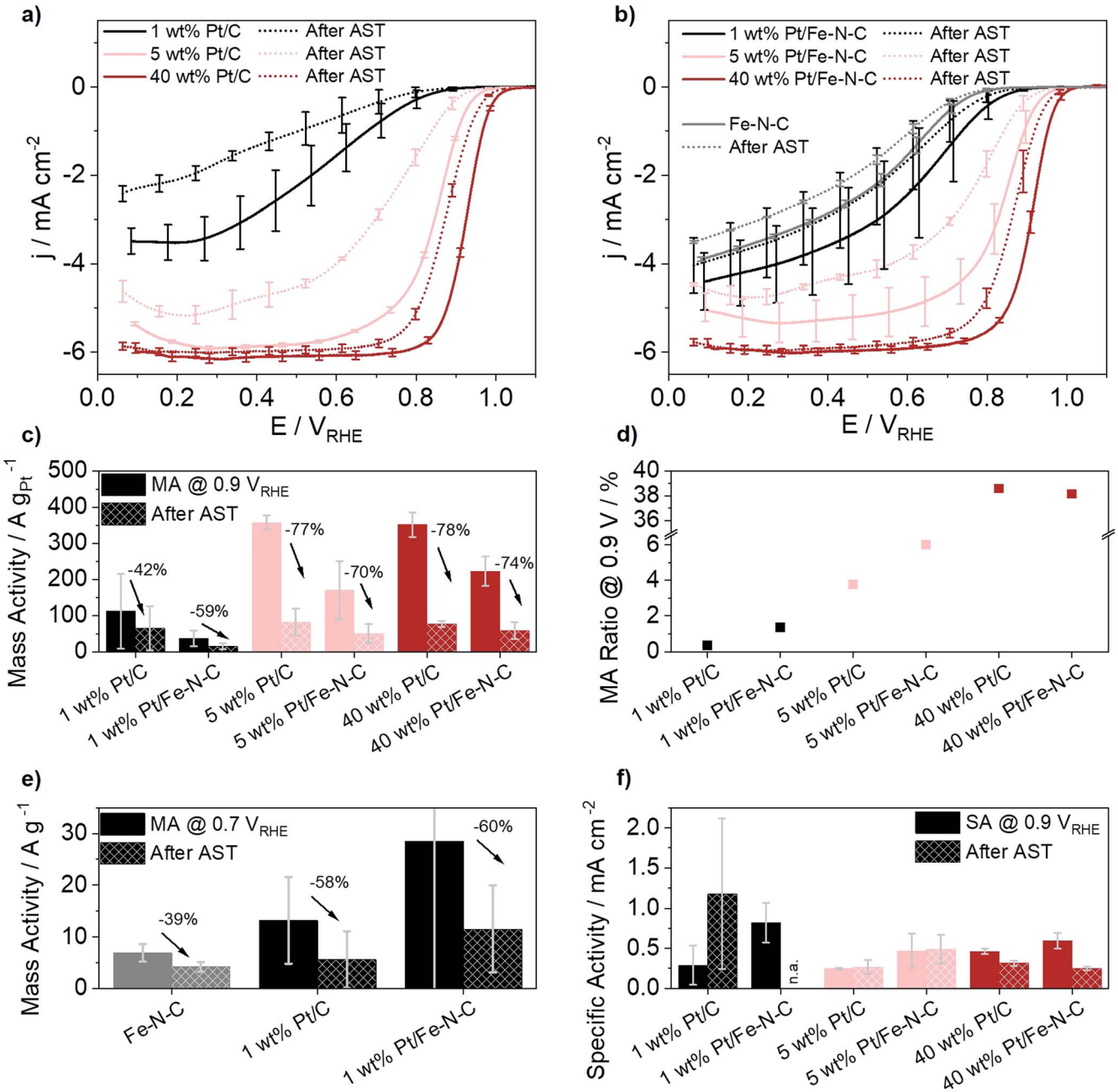

Figure 5. ORR polarization curves before and after AST (5,000 cycles, 0.6–1.5 V_{RHE} with 0.5 V s^{-1}, N_2-saturated $HClO_4$) of (a) Pt/C and (b) Pt/Fe-N-C catalysts at 1600 rpm with a scan rate of 5 mV s^{-1}, (c) mass activities at 0.9 V_{RHE} based on mass of platinum, (d) ratio of MA@0.9 V normalized by mass of Pt and MA@0.9 V normalized by mass of total catalyst, (e) mass activities at 0.7 V_{RHE} based on mass of total catalyst and f) specific activities at 0.9 V_{RHE} based on $ECSA_{CO}$.

XPS results on Pt are shown in Fig. 3, where Pt4f peaks have the main contribution of Pt^0 followed by minor contributions of oxidation states II and IV. Pt^0 peak positions are marked with dashed lines and reveal that the highest Pt mass fraction of 40 wt% leads to a negative shift of binding energy for both catalysts compared to the lower Pt content cases. This is due to higher occurrence of electronical Pt interaction among each other. Although Fig. 3 does not reveal an important impact of the support material on Pt^0 peak positions, small shifts become visible by comparing the peak maxima (Table SI). Electronic interaction of Pt with Fe-N-C leads to a slight positive shift with increased binding energy. Peak shifts are 0.09, 0.36 and 0.26 eV for 1, 5, 40 wt% Pt in case of $Pt^0 4f_{7/2}$ and 0.09, 0.51 and 0.11 eV for 1, 5, 40 wt% Pt in case of $Pt^0 4f_{5/2}$. A positive shift of 0.19 eV was also observed by Liao et al. and assigned to electronic N-/Pt-interaction.[17] This slight impact of Fe-N-C on Pt might consequences a difference in catalytic activity for ORR and/or electrochemical stability, which are investigated in detail below. Pt nanoparticles are known to be impacted by their preparation conditions that are kept constant in this study and by the environment of the particles.[27] Furthermore, Fig. 3 shows a difference in the Pt^{4+} fraction at low Pt contents of 5 wt% and 1 wt%. Pt^{4+} is more pronounced for Pt/Fe-N-Cs than for Pt/Cs (marked with arrows in Fig. 3; Table SII). Whereas this difference is not visible in case of the highest Pt content of 40 wt%, low amounts of Pt seem to be more influenced by the heteroatom sites in the Fe-N-C. It can be assumed, that low Pt amounts are precipitated on

Table II. ORR activities of Pt-based and M-N-C-based catalysts in comparison.

Catalyst	Pt content	Test conditions	Mass Activity (0.9 V)	References
		Pt-based catalysts		
PtCo/CNT	22.9 wt%	0.1 mol l^{-1} $HClO_4$, room temperature, 10 μg_{Pt} cm^{-2}, ORR at 900 rpm and 50 mV s^{-1}	311 A g_{Pt}^{-1}	4
Pt/C (Johnson Matthey)	20 wt%	0.1 mol l^{-1} $HClO_4$, room temperature, 20 μg_{Pt} cm^{-2}, ORR at 1600 rpm and 10 mV s^{-1}	~300 A g_{Pt}^{-1}	31
		M-N-C-based catalysts		
Hybrid Pt/Fe-N-C	~2.0 wt%	0.1 mol l^{-1} $HClO_4$, room temperature, 800 μg_{total} cm^{-2}, ORR at 1600 rpm and 10 mV s^{-1}	~0.3 A g_{total}^{-1}	16
Pt/Fe-N-C	1.4 wt%	0.1 mol l^{-1} $HClO_4$, room temperature, 2.7 μg_{Pt} cm^{-2}, ORR at 1600 rpm and 50 mV s^{-1}	420 A g_{Pt}^{-1}	17
NC-protected Fe-N-C	—	0.5 mol l^{-1} H_2SO_4, room temperature, 600 μg_{total} cm^{-2}, ORR at 900 rpm and 10 mV s^{-1}	10.3 A g_{total}^{-1}	13
		This study		
1 wt% Pt/C	0.4 wt%	0.1 mol l^{-1} $HClO_4$, room temperature, 100 μg_{total} cm^{-2}, ORR at 1600 rpm and 5 mV s^{-1}	112 A g_{Pt}^{-1} 0.4 A g_{total}^{-1}	
5 wt% Pt/C	3.8 wt%		356 A g_{Pt}^{-1} 14 A g_{total}^{-1}	
40 wt% Pt/C	38.6 wt%		352 A g_{Pt}^{-1}	
Fe-N-C (Pajarito Powder)	—		0.1 A g_{total}^{-1}	
1 wt% Pt/Fe-N-C	1.4 wt%		37 A g_{Pt}^{-1} 0.5 A g_{total}^{-1}	
5 wt% Pt/Fe-N-C	4.0 wt%		171 A g_{Pt}^{-1} 10 A g_{total}^{-1}	
40 wt% Pt/Fe-N-C	38.1 wt%		223 A g_{Pt}^{-1}	

and preferentially interact with these heteroatom sites of Fe-N-C. The higher occurrence of Pt^{4+} is not visible for Pt/Cs.

Figures S1 and 2 and Table SII show the further summarized XPS results on N1s, C1s, O1s and Fe2p. Fe-N-C based catalysts contain more nitrogen between 4.9–9.5 at% than carbon black based catalysts between 1.8–3.1 at% (Table SII). Among the Fe-N-C samples, there is no trend for single nitrogen species (pyridinic, pyrrolic, graphitic, nitroxide) from low (1 wt%) to high (40 wt%) amounts of precipitated Pt. Our previous study on same PMF type in comparison with further modified Fe-N-Cs for HT-PEMFC cathodes resulted in N contents of 5.4 at% for PMF, 6.0 at% for Fe-N-C based on Black Pearls® and 9.1–10.3 at% for biomass based Fe-N-Cs.[28] Other studies reported a N content in PMF of 2.7 at%[29] and 2.3 at%.[19] Regarding Fe2p, it is typical that peaks of Fe-N-Cs have a very low intensity due to low Fe amounts that does not allow a proper peak analysis (Fig. S2).[30] The used PMF in this study shows a bulk Fe concentration of 1.2 wt% determined by ICP-MS in our previous study.[28]

Catalyst activity and stability.—After physical characterization, the catalysts are electrochemically investigated towards their ECSA and activity for the ORR in $HClO_4$ electrolyte. These parameters are determined before and after accelerated stress testing to evaluate stabilities. Measurements are performed using perchloric acid, since the effect of Fe-N-C support for platinum activity and stability is investigated. Hu et al. compared electrochemical measurements of common Pt/C and Fe-N-C along different electrolytes and reported comparatively strong H_2SO_4 poisoning of Pt and the highest catalytic activity of Pt in $HClO_4$, whereas Fe-N-C showed stronger poisoning in case of $HClO_4$ but with less pronounced differences in the catalytic activity along these two electrolytes compared to Pt.[31] Figure 4 compares CV and CO stripping voltammetry curves and the corresponding ECSAs along all catalysts. Figures 4a and 4b reveal that faradaic and capacitive current densities recorded during cyclic voltammetry are lower for Pt/Fe-N-Cs than for Pt/Cs along all Pt content cases. Because total catalyst amounts on the electrodes are kept the same, this indicates lower electrode capacity of Pt/Fe-N-Cs on the one hand and lower electrochemical Pt nanoparticle availability on Fe-N-C (PMF) than on C (Black Pearls®) on the other hand. In previous investigations, we determined specific surface areas of 588 m^2g^{-1} (PMF)[28] and 1,518 $m^2\ g^{-1}$ (Black Pearls®). In case of both 1 wt% Pt catalysts the characteristic Pt peaks with hydrogen underpotential deposition (HUPD) are not detectable which was expected due to very low Pt content. It is according to TEM in Fig. 1 and ICP-MS in Table I. Therefore, ECSA calculation in Fig. 4e is not possible later. The CV curves in Figs. 4a and 4b after AST show HUPD peak decreases (approx. 0.05–0.3 V_{RHE}) and hydroquinone/quinone peaks increases (approx. 0.4–0.8 V_{RHE}), which is well-known for Pt catalyst degradation as well as carbon support degradation.[26,32–34]

Figures 4c and 4d depict the CO stripping curves and also show less pronounced CO oxidation peaks for Pt/Fe-N-Cs than for Pt/Cs along all Pt content cases in terms of CO oxidation. Another interesting trend in dependence on the Pt content gets obvious here for both supports likewise. Whereas the 1 wt% Pt catalysts show negligible peaks of CO oxidation, the 5 wt% and 40 wt% Pt catalysts show same trends in changing of peak shapes before and after AST. This seems independent of the C or Fe-N-C support. For 40 wt% Pt/C and Pt/Fe-N-C the peak shape changes from one symmetric signal before AST to three strongly overlapped main signals with much lower intensity than the initial signal. Peak maximums before AST are centered at 0.849 V_{RHE} for Pt/C and at 0.824 V_{RHE} for Pt/Fe-N-C. Peak maximums of the three signals after AST are at 0.751 V_{RHE}, 0.828 V_{RHE} and 0.890 V_{RHE} for Pt/C and at 0.729 V_{RHE}, 0.831 V_{RHE} and 0.926 V_{RHE} for Pt/Fe-N-C. These signals indicate typical Pt particle degradation in terms of agglomeration after AST[35] and show that the electrochemically provoked change of size, shape and surface of Pt particles is not influenced here by the supports to a larger extent. This shows a minor effect of carbon structure with incorporated Fe-N_x and N sites here. For 5 wt% Pt/C and Pt/Fe-N-C the peak shape changes from one signal to a very broad low intensity signal which might be the overlap of several peaks again. Peak maximums of 5 wt% Pt catalysts before AST are at 0.818 V_{RHE} for Pt/C and at 0.814 V_{RHE} for Pt/Fe-N-C. These very similar CO oxidation behavior with similar peak centers show again comparable size, shape and surface of Pt nanoparticles on both supports in comparison. This trend is expected due to the same catalyst preparation in this study, which includes a separate Pt nanoparticle synthesis first and the deposition on the support second.

ECSAs in Figs. 4e and 4f are calculated based on HUPD and CO stripping. In general, higher standard deviations for 5 wt% and 40 wt % Pt/Fe-N-Cs are observed compared to Pt/C which might be due to more inhomogeneous Pt nanoparticle distribution on the bulk support. Next to higher standard deviations, the $ECSA_{HUPD}$ and $ECSA_{CO}$ values are lower for Pt/Fe-N-Cs than for Pt/C along all Pt content cases. This proves the assumption of lower electrochemical Pt nanoparticle availability on Fe-N-Cs above and combines this assumption with a more inhomogeneous Pt availability on Fe-N-Cs. The 40 wt% Pt/C in this study has an $ECSA_{HUPD}$ value of 94 ± 5 $m^2\ g_{Pt}^{-1}$ and an $ECSA_{CO}$ value of 76 ± 8 $m^2\ g_{Pt}^{-1}$. It is in range of literature values ranging between 59–125 $m^2\ g_{Pt}^{-1}$.[36] The 40 wt% Pt/Fe-N-C in comparison has an $ECSA_{HUPD}$ value of 47 ± 14 $m^2\ g_{Pt}^{-1}$ and an $ECSA_{CO}$ value of 38 ± 8 $m^2\ g_{Pt}^{-1}$.

Although ECSAs of Fe-N-C supported Pt catalyst are lower here compared to C supported Pt catalyst, the Pt/Fe-N-Cs show lower loss of ECSA after AST and in consequence a better stability than Pt/Cs for 5 wt% and 40 wt% catalysts in CO stripping and for 40 wt% catalysts in HUPD. The determination of ECSAs in case of the low 1 wt% content catalysts is difficult and has low significance due to low peak intensities during CV.

Figure 5 compares the ORR curves as well as the mass and specific activities before and after AST. These curves and activities are shown for the three Pt/C catalysts and the three Pt/Fe-N-C catalysts with 1 wt%, 5 wt% and 40 wt% Pt contents. In addition, the platinum-free Fe-N-C catalyst only is shown to assess the ORR without the presence of platinum. Although Pt contents of 5 and 40 wt% highly differ from each other, Figs. 5a–5b demonstrate a potential shift in ORR curves of approx. 100 mV only. Thus, it is expected that ORR of deviating Pt contents between 5–40 wt% would appear in this narrow potential window. Also, mass activities of 5 and 40 wt% are very comparable in Fig. 5c.

While 40 wt% Pt/C and 40 wt% Pt/Fe-N-C show the expected diffusion limited current density of around −6 mA cm^{-2} which is typical for Pt catalysts in $HClO_4$, the others show a successive reducing trend of diffusion limited current densities dependent on the Pt content but independent of the support. Impact factors for this diffusion limited potential region below 0.6 V_{RHE} are uniformity of coverage of the electrode with catalyst material depending on different support morphologies and Pt loading, electrical conductivities and ORR mechanism.[37,38]

Next to the diffusion limited region, the region at higher potentials above around 0.6 V_{RHE} shows much lower current densities and is more dominated by catalytic activity than diffusion. Mass activities are calculated at 0.9 V_{RHE} for all Pt catalysts and compared in Fig. 5c. Trends along the catalysts similar to ECSAs in Figs. 4e and 4f are revealed. Mass activities of Pt/Cs are higher than activities of Pt/Fe-N-Cs in all cases. Pt/C (40 wt%) has a mass activity of 352 A g_{Pt}^{-1} which is comparable with literature values of commercial Pt/Cs (38–47 wt%) ranging between 200–650 A g_{Pt}^{-1}.[36] Although Pt nanoparticle interaction with heteroatom-containing sites like nitrogen was shown in other studies to enhance the ORR activity because of greater electron density,[39,40] this positive effect on MA is not visible for Pt/Fe-N-Cs here. A significant difference in MA losses after AST is not visible, although for 5 wt% and 40 wt% Pt these losses are slightly lower in presence of Fe-N-C. A better electrochemical stability for Pt/Fe-N-C hybrids was also reported by Xiao et al. and Mechler et al.[14–16]

Figure 5d considers the mass activities at 0.9 V_{RHE} normalized by mass of Pt from Fig. 5c and normalized by the mass of total catalysts including Pt and the support (Table SIII) and shows their ratios for each catalyst. The ratio visualizes the contribution of the total catalyst to the overall activity for ORR. If Fe-N-C is present, this ratio is higher for the low Pt cases of 1 wt% and 5 wt% and evidences the Fe-N-C contribution to the ORR. The ratio becomes larger with increasing Pt fraction and is close to 40% for the 40 wt% Pt catalysts, where the effect of Fe-N-C as catalytic active support becomes negligible and the main contribution to ORR stems from Pt itself.

Figure 5e shows mass activities at 0.7 V_{RHE} for the low content Pt catalysts compared to Fe-N-C only without deposited Pt based on the mass of total catalyst. Oxygen reduction starts at lower potentials for these catalysts than for the others because of larger overpotentials, so that a potential of 0.7 V_{RHE} is chosen for comparison here. Uncertainties in MA determination shown by errors bars here increase with decreasing Pt contents, since the main ORR activity stems from Pt and Pt inhomogeneities might play a role here. While Fe-N-C only shows a mass activity of 6.9 A g^{-1} (Table SIV), the mass activity for 1 wt% Pt/C is 13.2 A g^{-1} and for Pt/Fe-N-C 28.6 A g^{-1}. This illustrates that the use of Fe-N-C support for low Pt content catalysts instead of C only has a boosting effect on ORR activity by factor of two. After performing the stress testing, the loss of MA for 1 wt% Pt catalysts is 58%–60% and thus comparable. However, the loss of MA for Fe-N-C is lower and counts 39%, so that catalytic active Fe-N_x sites seem to be more stable than Pt sites for this AST.

Figure 5f shows the specific activities that are calculated based on $ECSA_{CO}$ instead of $ECSA_{HUPD}$. HUPD made the ECSA for 1 wt% Pt cases not accessible, while CO stripping is more sensitive for ECSA calculation. The initial SAs are higher for Pt/Fe-N-Cs in all cases, so that their activity with regard to the electrochemical Pt surface is higher. This can stem from additional contribution of Fe-N-C to ORR activity for low Pt content cases according to Fig. 5d. And this can further stem from a positive effect of Fe-N-C to the ORR activity of the electrochemical Pt surface, since a positive effect is also visible for 40 wt% Pt catalysts. Electronic impact of Fe-N-C on Pt was shown by XPS in Fig. 3. Regarding the investigation of stability here, the low Pt content cases of 1 wt% and 5 wt% show no loss of SA. For Pt contents of 40 wt% a loss of SA gets visible, that can result from typical Pt degradation like agglomeration (see CO stripping curves in Figs. 4b and 4c.

Table II summarizes and compares mass activities of this study with other selected studies in this research field. 1 wt% Pt/Fe-N-C shows a five times higher activity than the commercial Fe-N-C only (0.5 vs 0.1 A g_{total}^{-1}) and competes with the hybrid Pt/Fe-N-C from Mechler et al.[16] Even though the activity of NC-protected Fe-N-C from Liu et al. is twice as high,[13] the used H_2SO_4 electrolyte must be considered, which leads to less adsorption on Fe-N-C catalyst surface than $HClO_4$ and limits the comparison here.[31] The 40 wt% Pt/Fe-N-C shows lower Pt activity of around 1/3 compared to 40 wt% Pt/C from this study and Pt-based catalysts from the other studies, so that Pt activity does not benefit from the Fe-N-C support.

Conclusions

In this study, the deposition of fabricated Pt nanoparticles on a carbon black and on Fe-N-C in different amounts of 1, 5 and 40 wt% was shown. Although Pt nanoparticles were well-distributed on both support classes, electrochemical results revealed differences in Pt behavior on the supports. ECSAs and MAs of platinum were lower on Fe-N-C than on carbon black, so that Pt itself does not profit in any significant catalytic matter from interaction with Fe-N_x and N sites. After electrochemical stress testing, Pt degradation, visible during CO stripping voltammetry, was similar and not influenced by the supports to a larger extent. However, by considering the mass activities of the total catalyst consisting of Pt and support, the use of Fe-N-C instead of C had a boosting effect on ORR activity for the low Pt content cases of 1 wt% and 5 wt%. This effect became negligible using 40 wt% platinum, since the main contribution to ORR stems from Pt. For the 1 wt% Pt cases, an activity increase by factor of two is shown when Fe-N-Cs are used. This observation will lead to optimize further strategies for the reduction of Pt content without sacrificing catalyst activity in PEMFC performance. To conclude, the combination of catalytic active Pt with catalytic active Fe-N_x sites has a synergetic effect on the overall ORR activity at low Pt contents. In further approaches, these catalysts would be explored with an aim to reduce the Pt amounts of PEM-based cathodes in both fuel cell types.

Acknowledgments

This study is in frame of the project HT-PEM 2.0 with the grant number 03ETB016A funded by the Federal Ministry for Economic Affairs and Climate Action on the basis of a decision by the German Bundestag. The authors thank the Electron and Light Microscopy Service Unit of the School of Mathematics and Science of the Carl von Ossietzky University for the use of the imaging facilities and, moreover, Levi Laurenz Schlüschen (DLR) for support in synthesizing Pt nanoparticles. XPS measurements done by Indro S. Biswas (DLR) are appreciated.

ORCID

Dana Schonvogel https://orcid.org/0000-0002-2485-740X
Nambi Krishnan Nagappan https://orcid.org/0000-0002-3563-050X
Julia Müller-Hülstede https://orcid.org/0000-0001-7822-8425
Peter Wagner https://orcid.org/0000-0002-5644-9881

References

1. B. Martinez-Vazquez, D. G. Sanchez, J. L. Castillo, K. A. Friedrich, and P. L. Garcia-Ybarra, *Int. J. Hydrogen Energy*, **40**, 5384 (2015).
2. Y. Wang, D. Wang, and Y. Li, *SmartMat*, **2**, 56 (2021).
3. Z. Zhao, Z. Liu, A. Zhang, X. Yan, W. Xue, B. Peng, H. L. Xin, X. Pan, X. Duan, and Y. Huang, *Nat. Nanotechnol.*, **17**, 968 (2022).
4. N. Shroti and M. K. Daletou, *Int. J. Hydrogen Energy*, **47**, 16235 (2022).
5. T. Reshetenko, A. Serov, M. Odgaard, G. Randolf, L. Osmieri, and A. Kulikovsky, *Electrochem. Commun.*, **118**, 106795 (2020).
6. Y. He, S. Liu, C. Priest, Q. Shi, and G. Wu, *Chem. Soc. Rev.*, **49**, 3484 (2020).
7. Q. Meyer, C. Yang, Y. Cheng, and C. Zhao, *Electrochemical Energy Reviews*, **6**, 16 (2023).
8. F. Jaouen, D. Jones, N. Coutard, V. Artero, P. Strasser, and A. Kucernak, *Johnson Matthey Technol. Rev.*, **62**, 231 (2018).
9. U. Martinez, S. Komini Babu, E. F. Holby, H. T. Chung, X. Yin, and P. Zelenay, *Adv. Mater.*, **31**, 1806545 (2019).
10. K. Kumar, L. Dubau, M. Mermoux, J. Li, A. Zitolo, J. Nelayah, F. Jaouen, and F. Maillard, *Angew. Chem. Int. Ed.*, **59**, 3235 (2020).
11. G. Bae, S. Han, H. S. Oh, and C. H. Choi, *Angew. Chem.*, **135**, e202219227 (2023).
12. J. Müller-Hülstede, H. Schmies, D. Schonvogel, Q. Meyer, Y. Nie, C. Zhao, P. Wagner, and M. Wark, *Int. J. Hydrogen Energy*, **in press** (2023).
13. S. Liu et al., *Nat. Energy*, **7**, 652 (2022).
14. F. Xiao, G.-L. Xu, C.-J. Sun, I. Hwang, M. Xu, H.-W. Wu, Z. Wei, X. Pan, K. Amine, and M. Shao, *Nano Energy*, **77**, 105192 (2020).
15. F. Xiao, Q. Wang, G.-L. Xu, X. Qin, I. Hwang, C.-J. Sun, M. Liu, W. Hua, H.-W. Wu, and S. Zhu, *Nat. Catal.*, **5**, 503 (2022).
16. A. K. Mechler, N. R. Sahraie, V. Armel, A. Zitolo, M. T. Sougrati, J. N. Schwämmlein, D. J. Jones, and F. Jaouen, *J. Electrochem. Soc.*, **165**, F1084 (2018).
17. W. Liao, S. Zhou, Z. Wang, F. Liu, H. Pan, T. Xie, and Q. Wang, *ChemCatChem*, **13**, 4925 (2021).
18. J. Müller-Hülstede, L. M. Uhlig, H. Schmies, D. Schonvogel, Q. Meyer, Y. Nie, C. Zhao, J. Vidakovic, and P. Wagner, *ChemSusChem*, **16**, e202202046 (2023).
19. M. Primbs et al., *Energy Environ. Sci.*, **13**, 2480 (2020).
20. R. Z. Snitkoff-Sol, A. Friedman, H. C. Honig, Y. Yurko, A. Kozhushner, M. J. Zachman, P. Zelenay, A. M. Bond, and L. Elbaz, *Nat. Catal.*, **5**, 163 (2022).
21. Y. Wang, J. W. Ren, K. Deng, L. L. Gui, and Y. Q. Tang, *Chem. Mater.*, **12**, 1622 (2000).
22. R. Kou et al., *J. Am. Chem. Soc.*, **133**, 2541 (2011).
23. M. Inaba, J. Quinson, J. R. Bucher, and M. Arenz, *Jove-J Vis Exp* (2018).
24. D. Schonvogel, J. Hulstede, P. Wagner, I. Kruusenberg, K. Tammeveski, A. Dyck, C. Agert, and M. Wark, *J. Electrochem. Soc.*, **164**, F995 (2017).
25. A. Dushina, H. Schmies, D. Schonvogel, A. Dyck, and P. Wagner, *Int J Hydrogen Energ*, **45**, 35073 (2020).

26. D. Schonvogel, J. Hülstede, P. Wagner, A. Dyck, C. Agert, and M. Wark, *J. Electrochem. Soc.*, **165**, F3373 (2018).
27. L. K. Ono, B. Yuan, H. Heinrich, and B. R. Cuenya, *J. Phys. Chem. C*, **114**, 22119 (2010).
28. J. Müller-Hülstede, T. Zierdt, H. Schmies, D. Schonvogel, Q. Meyer, C. Zhao, P. Wagner, and M. Wark, *J. Power Sources*, **537**, 231529 (2022).
29. C. L. Vecchio, A. Serov, M. Dicome, B. Zulevi, A. Aricò, and V. Baglio, *Electrochim. Acta*, **394**, 139108 (2021).
30. A. Ghosh, S. Ghosh, G. M. Seshadhri, and S. Ramaprabhu, *Sci Rep.*, **9**, 5187 (2019).
31. Y. Hu, J. O. Jensen, C. Pan, L. N. Cleemann, I. Shypunov, and Q. Li, *Appl. Catal. B - Environ.*, **234**, 357 (2018).
32. D. Schonvogel, J. Hülstede, P. Wagner, I. Kruusenberg, K. Tammeveski, A. Dyck, C. Agert, and M. Wark, *J. Electrochem. Soc.*, **164**, F995 (2017).
33. K. Kinoshita and J. Bett, *Carbon*, **11**, 237 (1973).
34. J. Speder, A. Zana, I. Spanos, J. J. K. Kirkensgaard, K. Mortensen, and M. Arenz, *Electrochem. Commun.*, **34**, 153 (2013).
35. S. Taylor, E. Fabbri, P. Levecque, T. J. Schmidt, and O. Conrad, *Electrocatalysis*, **7**, 287 (2016).
36. S. S. Kocha, K. Shinozaki, J. W. Zack, D. J. Myers, N. N. Kariuki, T. Nowicki, V. Stamenkovic, Y. J. Kang, D. G. Li, and D. Papageorgopoulos, *Electrocatalysis-Us*, **8**, 366 (2017).
37. K. J. J. Mayrhofer, D. Strmcnik, B. B. Blizanac, V. Stamenkovic, M. Arenz, and N. M. Markovic, *Electrochim. Acta*, **53**, 3181 (2008).
38. G. Cognard, G. Ozouf, C. Beauger, I. Jiménez-Morales, S. Cavaliere, D. Jones, J. Rozière, M. Chatenet, and F. Maillard, *Electrocatalysis*, **8**, 51 (2017).
39. D. R. Kauffman and A. Star, *Analyst*, **135**, 2790 (2010).
40. M. N. Groves, A. S. W. Chan, C. Malardier-Jugroot, and M. Jugroot, *Chem. Phys. Lett.*, **481**, 214 (2009).